Effects of Displacement and Rate Saturation on the Control of Statically Unstable Aircraft

Gregory D. Hanson* and Robert F. Stengel†
Princeton University, Princeton, New Jersey

Methodologies are presented for the analysis and design of stability augmentation control laws for aircraft in which "hard" displacement and rate limiting are significant. Candidate control laws are derived using the linear-quadratic (LQ) regulator. Analytical and computational estimates of the stability limits imposed by control saturation are presented using state trajectories, as well as describing functions and eigenvalue computation. Analysis also includes an investigation of the interaction of the state-space saturation and stability boundaries for various choices of LQ weighting matrices. For minimum energy control, the saturation and stability boundaries are shown to be parallel. In this case, there is a direct relation between the solution to the matrix Riccati equation and the aircraft's open-loop dynamics.

VIRTUALLY all aircraft control system actuation mechanisms possess "hard" limits on deflection and rate of deflection, and accounting for these limits is particularly important for aircraft designed with relaxed or negative static stability. Relaxed static stability generally leads to reduced weight and trim drag, both of which enhance the aircraft's performance.[1] Relaxed static stability also may lead to increased control activity.[2] For such aircraft, consideration must be given to the effects of control saturation on the initiation and, more importantly, the arrestment of dynamic motions, if departure from controlled flight is to be prevented. It may be possible to provide hardware actuation limits large enough so that normal disturbances and command inputs do not force the controls and to their mechanical, hydraulic, or electrical "stops"; however, there is no guarantee that commanded control deflections or rates will not exceed any established limit. Therefore, it is important to define the region within which stability and satisfactory response can be assured.

This paper explores the effects of deflection and rate saturation on the stability of a statically unstable aircraft. This paper also reports on the development of methodologies for the analysis and design of stability augmentation control laws, with emphasis on response to initial conditions. (Command response is presented in Ref. 3 is the subject of a separate paper.[11]) Candidate stability augmentation system (SAS) control laws are derived using optimal control theory, with the linear-quadratic (LQ) regulator taken as the fundamental solution. Analytical and computational estimates of the stability limits imposed by control saturation are presented.

Modeling Approach

The longitudinal equations of motion for a generic lightweight fighter aircraft are chosen as a baseline for study.[4] They are linearized as

$$\Delta\dot{x} = F\Delta x + G\Delta\delta \tag{1}$$

where the state vector Δx contains axial and normal velocities, pitch rate, and pitch angle.

$$\Delta x = [\Delta u\ \Delta w\ \Delta q\ \Delta\theta]^T \tag{2}$$

The control vector $\Delta\delta$ contains elevator and throttle positions,

$$\Delta\delta = [\Delta\delta E\ \Delta\delta T]^T \tag{3}$$

and the system matrices are assumed to take the form,

$$F = \begin{bmatrix} X_u & X_w & (X_q - w_0) & -g\cos\theta_0 \\ Z_u & Z_w & (Z_q + u_0) & -g\sin\theta_0 \\ M_u & M_w & M_q & 0 \\ 0 & 0 & 1 & 0 \end{bmatrix} \tag{4}$$

$$G = \begin{bmatrix} 0 & X_{\delta T} \\ 0 & 0 \\ M_{\delta E} & 0 \\ 0 & 0 \end{bmatrix} \tag{5}$$

The level-flight trim condition was specified at an altitude of 20,000 ft with a true airspeed of 700 ft/s. The aircraft was configured with a statically *unstable* center-of-gravity (c.g.) location; the c.g. was assumed to be aft of the neutral point by 20% of the mean aerodynamic chord, yielding

$$F = \begin{bmatrix} -0.036 & 0.1039 & -0.947 & -0.560 \\ -0.024 & -0.873 & 12.18 & -0.046 \\ -0.061 & 0.784 & -0.777 & 0 \\ 0 & 0 & 1.0 & 0 \end{bmatrix} \tag{6}$$

Presented as Paper 81-1752 at the AIAA Guidance and Control Conference, Albuquerque, N. Mex., Aug. 19-21, 1981; submitted Sept. 30, 1981; revision received June 7, 1983.

*Formerly Graduate Student, Department of Mechanical and Aerospace Engineering, Flight Research Laboratory. Currently Engineer, Systems Technology, Inc., Mountain View, Calif. Student Member AIAA.

†Professor of Mechanical and Aerospace Engineering, Flight Research Laboratory. Associate Fellow AIAA.

$$G=\begin{bmatrix} 0 & 14.51 \\ 0 & 0 \\ -7.215 & 0 \\ 0 & 0 \end{bmatrix} \tag{7}$$

The numerical values assume that velocities and angles are measured in feet per second and degrees, respectively, while the throttle setting is measured in percent of maximum travel.

Control-displacement saturation effects on aircraft response are considerd using the fourth-order linear model. Control-rate limiting effects on aircraft response are considered most easily by redefining the state and control vectors. The state vector Δx is augmented to include control positions

$$\Delta x_R = [\Delta x \; \Delta\delta]^T \tag{8}$$

Control rates become the commanded variables,

$$\Delta\delta_R = [\Delta\dot{\delta}]^T \tag{9}$$

and the system matrices are defined to be

$$F_R=\begin{bmatrix} F & G \\ 0 & 0 \end{bmatrix} \tag{10}$$

$$G_R=\begin{bmatrix} 0 \\ I \end{bmatrix} \tag{11}$$

An elevator displacement limit of ± 20 deg is considered, and an elevator rate limit of $\Delta\dot{\delta}E = \pm 50$ deg/s is chosen for rate-limiting calculations.

Closed-Loop Control Laws: Stability Augmentation

Stability augmentation system (SAS) control laws are obtained using linear-quadratic (LQ) control theory. The optimal regulator is a linear feedback control law which minimizes a cost function:

$$J=\frac{1}{2}\int_0^\infty \{\Delta x^T Q \Delta x + \Delta\delta^T R \Delta\delta\}\,dt \tag{12}$$

The state-weighting matrix, Q, is symmetric and positive semidefinite, while the control weighting matrix, R, is positive definite and symmetric. The quadratic cost function is minimized subject to the dynamic constraint

$$\Delta\dot{x} = F\Delta x + G\Delta\delta \tag{13}$$

The optimal control law takes the form

$$\Delta\delta(t) = -C\Delta x(t) \tag{14}$$

The feedback gain matrix, C, is defined by

$$C = R^{-1}G^T P \tag{15}$$

where P satisfies the algebraic matrix Riccati equation,

$$-PF - F^T P + PGR^{-1}G^T P - Q = 0 \tag{16}$$

Substituting the control law [Eq. (13)], the optimal closed-loop dynamics become

$$\Delta\dot{x}(t) = (F - GC)\Delta x(t) \tag{17}$$

Since the reference aircraft is configured to possess a short-period static instability, it is of crucial importance that the candidate feedback controllers provide closed-loop stability. In order for the control system to be stable, the real parts of all of the eigenvalues of the closed-loop matrix $(F-GC)$ must be negative. There exist many solution matrices which satisfy Eq. (16) for given weighting matrices Q and R; however, a unique nonnegative definite solution matrix P is required and exists.[5]

It appears that linear-quadratic control theory provides a well-organized and acceptable design procedure for feedback control system design. However, there is no guarantee that large control deflections or rates will not be commanded. If Δx is large enough, control commands can exceed any established limit. The main objective of this study is to determine the region(s) of stable and satisfactory response for saturated LQ control of an open-loop unstable aircraft.

The stability augmentation system for control-rate saturation uses the redefined system variables described earlier [Eqs. (8-11)]. The zero set-point regulator for the latter is

$$\Delta\delta_R(t) = -C_x\Delta x(t) - C_{\dot{\delta}}\Delta\delta(t) \tag{18}$$

The feedback gain matrices C_x and $C_{\dot{\delta}}$ result from minimizing the cost function,

$$J=\frac{1}{2}\int_0^\infty \{[\Delta x^T \Delta\delta^T] Q_R \begin{bmatrix} \Delta x \\ \Delta\delta \end{bmatrix} + \Delta\dot{\delta}^T R_R \Delta\dot{\delta}\}\,dt \tag{19}$$

$$\Delta\dot{x}_R = R_R\Delta x_R + G_R\Delta\delta_R \tag{20}$$

with $x_R \triangleq [\Delta x \Delta\delta]^T$, $\Delta\delta R \triangleq \Delta\dot{\delta}$, and,

$$Q_R=\begin{bmatrix} Q & 0 \\ 0 & R \end{bmatrix} \tag{21}$$

$$R_R \equiv \text{Control-rate weighting} \tag{22}$$

Analytical Approach

This section treats the analysis of saturated LQ control. The numerical results presented here strictly apply only to the specific configuration studied; hence, care should be taken in generalizing these results to other configurations.

Control Displacement Limiting

The analysis proceeds along two separate lines. The first approach is to assess the nature of the instability, as reflected by the eigenvalues and eigenvectors, and to determine any resulting equilibrium (singular) points. The second approach is to derive candidate LQ feedback controllers and to assess the stability limits imposed for each controller. A single state-weighting matrix is chosen, and the LQ control laws are evaluated for various control weightings.

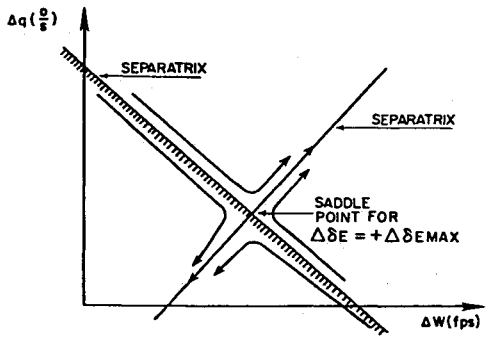

Fig. 1 Saddle-point trajectories.

State Trajectories

The open-loop eigenvalues of the fourth-order model characterize the aircraft's short-period and phugoid modes as

$$(\lambda_{sp_1}, \lambda_{sp_2}) = (-3.93, 2.28) \tag{23}$$

$$(\lambda_{p_1}, \lambda_{p_2}) = (-0.016, \pm 0.065i) \tag{24}$$

The subscripts *sp* and *p* are associated with the short-period and phugoid modes, respectively, and $i=(-1)^{1/2}$. The short-period mode is described by the two real eigenvalues; one is negative and stable, while the other is positive and unstable. The phugoid mode is oscillatory and stable.

A second-order model of the short-period mode illustrates the nature and location of the equilibrium points in the Δq-Δw state space. The second-order equations of the normal velocity and pitch rate are

$$\Delta\dot{w} = Z_w \Delta w + Z_q \Delta q \tag{25}$$

$$\Delta\dot{q} = M_w \Delta w + M_q \Delta q + M_{\delta E} \Delta\delta E \tag{26}$$

Equilibrium points for a second-order system can be classified according to the system's eigenvalues.[6] The equilibrium point associated with real eigenvalues of opposite sign is referred to as a *saddle point*. The location of the short-period saddle point is defined by the condition that $\Delta\dot{q}=\Delta\dot{w}=0$, i.e., $dq/dw=0/0$. Denoting the location of the equilibrium point by Δq^* and Δw^*, the simultaneous solution to Eqs. (25) and (26) for the left side equal to zero gives

$$\Delta w^* = (Z_q M_{\delta E} \Delta\delta E) / (Z_w M_q - M_w Z_q) \tag{27}$$

$$\Delta q^* = -(Z_w M_{\delta E} \Delta\delta E) / (Z_w M_q - M_w Z_q) \tag{28}$$

The location of the equilibrium point is seen to be a function of the control setting, $\Delta\delta E$. Thus, the saddle point on the stability boundary is determined by the solution to Eqs. (27) and (28), with $\Delta\delta E = +\Delta\delta E = +\Delta\delta E_{\max}$. The equilibrium points are actually intersections of higher dimensional *equilibrium lines* with the Δq-Δw plane.

Particular trajectories enter the saddle point and separate the state space into regions of distinct motion. Such trajectories are called *separatrices,* and they are shown in Fig. 1. In this system, one of the separatrices divides the state into two regions of distinct motion. The state-space trajectories show the initial condition response. If the initial point falls within the hatched region, the trajectories are directed toward the origin. With stabilizing control, the origin is a *stable focus* which captures the trajectory. If the initial point is outside the hatched region, the control remains saturated, and the trajectories grow without bound as time increases.

The separatrices represent the normal coordinate axes of the saddle point. The modal matrix of the system defines the slopes of the separatrices in the state space using the following procedures.

1) Determine the eigenvalues and eigenvectors of the unstable system $(\boldsymbol{F}, \boldsymbol{G})$. The eigenvalues are given by solving for λ_i such that the determinant,

$$|\lambda \boldsymbol{I} - \boldsymbol{F}| = 0 \tag{29}$$

and the eigenvectors, η_i, are given by

η_i = column of adj $(\lambda_i \boldsymbol{I} - \boldsymbol{F})$ $\quad i=1,2,3,\ldots,n$ where n is the order of the system.

2) Find the modal matrix, $\boldsymbol{M}$, which is given by adjoining the columns of η_i,

$$\boldsymbol{M} = [\eta_1 \eta_2 \ldots \eta_n] \tag{31}$$

3) The transform of the original coordinates to the normal coordinates, Δy of the saddle point is given by

$$(\Delta x - \Delta x^*) = \boldsymbol{M}(\Delta y - \Delta y^*) \tag{32}$$

where the starred quantities refer to the saddle-point location.

4) The normal coordinates of the saddle point are expressed in terms of the state coordinates as

$$(\Delta y - \Delta y^*) = \boldsymbol{M}^{-1}(\Delta x - \Delta x^*) \tag{33}$$

Setting the left-hand side of Eq. (33) equal to zero and solving for one state in terms of the others determines the slope of the separatrix in the state space. Since the separatrices pass through the saddle point, the equations of the separatrices are completely determined.

For the second-order system, the slopes of the separatrices in the Δq-Δw plane are

$$(\Delta q - \Delta q^*)/(\Delta w - \Delta w^*) = \tfrac{1}{2} Z_q \{ M_q - Z_w - [(M_q - Z_w)^2 + 4 M_w Z_q]^{1/2} \} \tag{34}$$

for $(\Delta y_1 - \Delta y_1^*) = 0$, and,

$$(\Delta q - \Delta q^*)/(\Delta w - \Delta w^*) = \tfrac{1}{2} Z_q \{ M_q - Z_w + [(M_q - Z_w)^2 + 4 M_w A_q]^{1/2} \} \tag{35}$$

for $(\Delta y_2 - \Delta y_2^*) = 0$.

The separatrices of the saddle point of the second-order system are completely defined by Eqs. (27), (28), (34), and (35), determining the initial condition stability boundary in the Δq-Δw plane, as indicated in Fig. 1.

Describing Function Analysis

The initial condition stability boundary imposed on saturating LQ feedback control also was estimated using a describing function analysis to predict the limiting values of state feedback. Although the precise quasilinear relationship between the describing function's input and output depends upon the waveform (e.g., a sinusoidal, random, or transient signal), the trends in the saturation describing function are the same in all cases—the larger the input signal, the greater the quasilinear attenuation.[7] The LQ regulator is guaranteed to retain asymptotic stability for loop-gain attenuation of 50% or more.[8]

Numerical results illustrated that a relationship such as

$$|E| = \Delta\delta E_{\max} / \rho_s \tag{36}$$

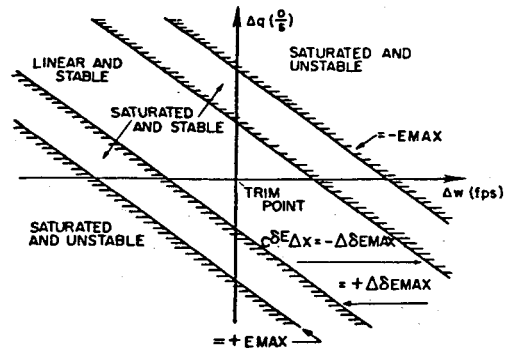

Fig. 2 State-space stability boundaries suggested by describing function analysis. Control deflection ($\Delta\delta E$) is constant.

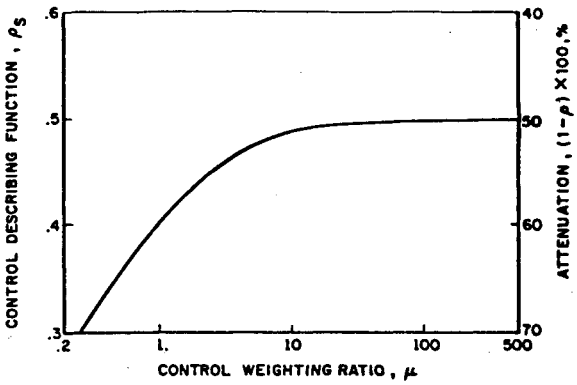

Fig. 3 Stability boundary predicted by describing function analysis as a function of linear-quadratic control weighting, μR. Aircraft model described by Eqs. (5) and (6); Q defined by Eq. (46).

where ρ_s is the corresponding describing function magnitude for neutral stability (as determined by eigenvalue analysis), appears to be appropriate. A suitable expression for the describing function ρ_s (in terms of the initial control E and $\Delta\delta E_{\max}$) remains to be determined. Nevertheless, we can formulate a concept for defining state-space stability boundaries in terms of the saturation describing function.

1) Given the unstable system (F,G), and the single control limit, $\Delta\delta E_{\max}$, it is assumed that the commanded control, $\Delta\delta E_c$, stabilizes the system for $|\Delta\delta E_c| < \Delta\delta E_{\max}$.

2) $\Delta\delta E_c$ is some feedback function of the system state. In the case of the LQ regulator feedback control, $\Delta\delta E_c = -C^{\delta E}\Delta x$, where $C^{\delta E}$ is the row of the total gain matrix, C, associated with elevator control, defined in Eq. (14).

3) $\Delta\delta E_c = \text{const} = -C^{\delta E}\Delta x$ defines a *hyperplane* in the state space.

4) For the LQ regulator, control is linear and stable between the two hyperplanes $\mp C^{\Delta E}\Delta x = \Delta E_{\max}$.

5) ρ_s is the corresponding describing function magnitude for neutral stability, as determined by eigenvalue computation. Alternatively, it expresses the gain attenuation tolerance of the LQ regulator. The describing function magnitude, together with $\Delta\delta E_{\max}$, specifies a limiting value of the initial control $|E|$ as in Eq. (36).

6) For the LQ regulator, control may saturate but remain stable between the two hyperplanes

$$\mp C^{\delta E}\Delta x = |E_{\max}(\rho_s, \Delta\delta E_{\max})| > \Delta\delta E_{\max} \tag{37}$$

The concept is illustrated by a sketch of the intersections of these hyperplanes with the Δq-Δw plane, Fig. 2. The eigenvalue analysis makes no distinction regarding the relationship between ρ_s, $E_{\max}$, and $\Delta\delta E_{\max}$; it merely predicts a limiting value of loop-gain attenuation. The control law defines the state-space hyperplane corresponding to given values of control setting. Saturation hyperplanes and stability hyperplanes must be parallel for a given control law (i.e., derived from a given set of weighting matrices), since they differ only by a constant, and the same feedback control law is used to define all control settings. The describing function formulation positions the $\pm E_{\max}$ hyperplanes relative to the $\pm\Delta\delta E_{\max}$ hyperplanes.

Control deflection ($\Delta\delta E$) is constant on each hyperplane, $C^{\Delta E}\Delta x = \text{const}$. The control saturation describing function could be interpreted as an amplitude-dependent describing function; hence, the actual control becomes

$$\Delta\delta(t) = -\rho C\Delta x(t) \tag{38}$$

where the loop-gain factor ρ varies from 0 to 1. The value of ρ_s is a function of the control law, which, in turn, depends upon the state- and control-weighting matrices in the quadratic cost function.

The sensitivity of ρ_s to control-weighting variations was evaluated by uniformly varying the elements of R and computing the closed-loop eigenvalues as ρ varies from 0 to 1. In other words, the R of Eq. (12) was replaced by μR and μ ranged from 0.25 to 10^4 with $\mu = 1$. The diagonal elements of R represented inverse elevator and throttle variances of $(20)^2$ deg^2 and $(2)^2$ percent,^{2} respectively. The Q matrix was held constant at

$$Q = \text{diag}\,[0.25\times10^{-7}\ 0.25\times10^{-4}\ \ 0.25\times10^{-4}\ 0.25\times10^{-4}] \tag{39}$$

A plot of the relationship between ρ_s and μ for this problem is given in Fig. 3. In effect, the describing function analysis indicates that small values of μ lead to small values of ρ_s at the stability boundary, i.e., to greater attenuation of control effects. As μ becomes larger, ρ_s limits at 0.5; high control weighting leads to minimum control energy solutions, which, nevertheless, possess the factor of two stability tolerance mentioned earlier.

While this may appear to imply that low control weighting provides large tolerance to saturation effects, such is not the case, because low control weighting also leads to higher feedback gains; therefore, saturation occurs at lower levels of the state feedback. Table 1 presents the elevator feedback gains, $C^{\delta E}$, for several values of μ and the implied limit on $\Delta\delta E$ standard deviation, $\sigma_{\delta E}$. (Throttle gains also are computed but are not germane to the discussion of elevator saturation.) The control laws approach the minimum control energy solution as μ approaches infinity. Note that the normal velocity gain C_w, which accounts for static instability introduced by negative static margin, decreased with increasing values of μ.

The limiting values for state feedback can now be predicted using Fig. 3 and Table 1. The feedback value of Δw which alone would saturate the elevator is

$$\Delta w_{\text{sat}} = \pm\Delta\delta E_{\max}/C_w \tag{40}$$

Hence, for $\Delta\delta E_{\max} = 20$ deg and $\mu = 0.25$, the normal velocity which causes saturation is 78.9 ft/s. Increasing μ to 100 increases Δw_{sat} to 127.5 ft/s. Figure 3 indicates that with $\mu = 0.25$, a 70% gain attenuation factor ($\rho_s = 0.3$) is required to produce neutral stability, while only 50% attenuation is allowed with $\mu = 100$ ($\rho_s = 0.15$). Assuming for the moment that Eq. (4) relates ρ_s to the limiting commanded control, $E_{\max}$ is 66.7 deg for $\mu = 0.25$, and it equals 40 deg for $\mu = 100$. From Table 1, the corresponding values of Δw, with the other state components equal to zero, are 263 and 255 ft/s, respectively. Performing the same calculations for the limiting values of Δq, predicts values of 76.3 and 63.4 deg/s,

Table 1 Elevator rate gains for various levels of control weighting,

μ	$\sigma_{\delta E}$, deg	C_u, deg/(ft/s)	C_w deg/(ft/s)	C_q deg/deg/s	C_θ, deg/deg
0.25	40.0	0.0116	−0.2536	−0.8731	−0.1839
1.0	20.0	0.0143	−0.1882	−0.7195	−0.0840
6.24	8.0	0.0170	−0.1622	−0.6487	−0.0239
25.0	4.0	0.0179	−0.1580	−0.6356	−0.0082
100.0	2.0	−0.0182	−0.1569	−0.6320	−0.0032
10^4	0.2	0.0183	−0.1565	−0.6308	−0.0014

Table 2 Elevator rate gains for various levels of control rate weighting, μ

μ	C_u	C_w	C_q	C_θ	$C_{\delta E}$	$C_{\delta T}$
0.1	0.0915	−0.9874	−3.954	−0.2652	8.189	0.2074
1.0	0.0588	−0.5685	−2.296	−0.0838	5.842	0.2074
10.0	0.0476	−0.4292	−1.733	−0.0266	5.011	0.2097
50.0	0.0445	−0.3914	−1.579	−0.0121	4.775	0.2147
100.0	0.0437	−0.3820	−1.540	−0.0087	4.715	0.2312
500.0	0.0427	−0.3684	−1.485	−0.0046	4.629	0.2312

respectively. Consequently, while describing function analysis predicts virtually the same limiting values of Δw feedback for both control laws, the same limiting values are not as closely predicted for Δq feedback. This implies a possibility of more than one stability boundary (depending upon the control law), but the calculation of time histories illustrates that the limiting values are not "virtually" the same, they are *exactly* the same for the two control laws and the actual control displacement saturation. This will be shown in a following section.

It is of interest to examine the relationship between the constant control saturation hyperplanes and the control weighting matrix. Table 1 illustrates that the constant control hyperplanes for various levels of μ are not parallel. Each hyperplane's slope in the intersecting state plane is defined by the ratio of the control gains. It follows that if there is a single stability boundary for two control laws, it can be parallel (at most) to no more than one law's control saturation hyperplane. It is shown below that the stability boundary is parallel to the saturation hyperplane for the minimum control energy LQ control law.

Asymptotic LQ Solution

Reference has been made to the specific case of the "minimum control energy" (MCE) LQ regulator, and it has been noted that this solution determines the limiting values of state feedback using the formulated describing function. As the control weighting matrix approaches infinity, the cost of control increases, and a MCE solution is obtained in the limit. If the aircraft is stable, the MCE solution is no control at all; C approaches zero. Since we are interested in a statically unstable aircraft, the feedback gains cannot go to zero and still guarantee a stable system; it is this nonzero asymptotic solution which is related to the open-loop characteristics of the aircraft.

In the limit, the control saturation and stability boundaries are parallel for both displacement and rate limiting. This is significant because unsaturated control guarantees stability when saturation and stability boundaries are parallel. This is shown using the same reduced-order models that were used to predict the saddle-point separatrices. Only the major results for displacement limiting are included here; a more complete discussion, including command response and similar results for rate limiting can be found in Ref. 3.

Consider the second-order model described by Eqs. (25) and (26) and an LQ regulator with scalar control, $\Delta\delta E$, Eq. (4). We are concerned with the properties of this regulator as a function of the weights $\boldsymbol{Q}$ and $\boldsymbol{R}=\beta r$, as β approaches infinity.

The control law that minimizes the cost function is given by

$$\Delta\delta_2(t) = -(\beta r)^{-1}\boldsymbol{G}_2^T\boldsymbol{P}\Delta\boldsymbol{x}(t) \tag{41}$$

where $\boldsymbol{P}$ is the steady-state solution matrix to the algebraic Riccati equation

$$-\boldsymbol{P}\boldsymbol{F}_2 - \boldsymbol{F}_2^T\boldsymbol{P} + \boldsymbol{P}\boldsymbol{G}_2(\beta r)^{-1}\boldsymbol{G}_2^T\boldsymbol{P} - \boldsymbol{Q} = 0 \tag{42}$$

The solution to Eq. (42), as β approaches infinity in the limit, yields the minimum control energy feedback gains; hence, it determines the control saturation boundary. The feedback gain matrix, $\boldsymbol{C}_2$, is given by

$$\boldsymbol{C}_2 = (\beta r)^{-1}\boldsymbol{G}_2^T\boldsymbol{P} \tag{43}$$

The slope of the saturation boundary is

$$-C_w/C_q = -p_{12}/p_{22} \tag{44}$$

where p_{12} and p_{22} are the MCE elements of the steady-state $\boldsymbol{P}$ matrix.

Substituting the appropriate matrices into Eq. (42), the ratio of p_{12}/p_{22} in the limit is

$$p_{12}/p_{22} = -M_q/Z_q + (p_{22}/\beta)(M_{\delta E}^2/2rZ_q) \tag{45}$$

Only the value of p_{22}/β is needed to define the slope of the MCE saturation boundary.

Reducing the scalar equations obtained from Eq. (42) to a single equation for p_{22}/β gives a fourth-order equation with the following roots:

$$(p_{22}/\beta)_1 = 0 \tag{46}$$

$$(p_{22}/\beta)_2 = (M_q + Z_w)\,2r/M_{\delta E}^2 \tag{47}$$

$$(p_{22}/\beta)_3 = \{M_q + Z_w + [(M_q - Z_w)^2 + 4M_wZ_q]\}r/M_{\delta E}^2 \tag{48}$$

$$(p_{22}/\beta)_4 = \{M_q + Z_w - [(M_q - Z_w)^2 + 4M_wZ_q]\}r/M_{\delta E}^2 \tag{49}$$

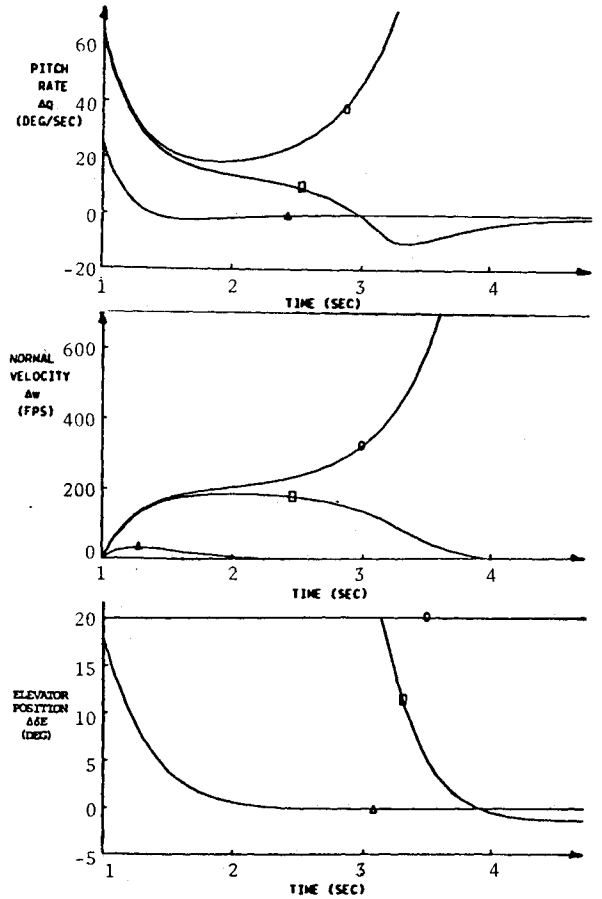

Fig. 4 Response to pitch rate initial conditions (control displacement limiting).

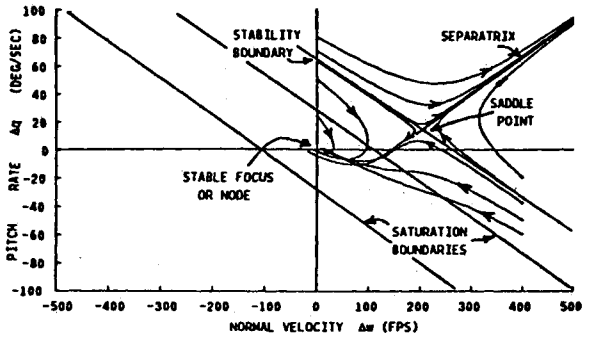

Fig. 5 Projections of state-space trajectories on the Δw-Δw plane (control displacement limiting).

It is seen that as β approaches infinity, one solution for p_{22}/β is zero. This would be the MCE LQ solution if F was stable. For F containing unstable eigenvalues the correct choice of p_{22}/β is determined by the root that yields a nonnegative definite P matrix. For minimum control energy, these equations give an easy closed-form detemination of the steady-state P matrix, as well as the feedback gains. However, what is more important is that the possible solutions are directly related to the open-loop characteristics of the second-order system.

This relationship to the open-loop system is seen by examining the characteristic equation of the second-order system. The characteristic equation is

$$\lambda^2-(M_q+Z_w)\lambda+(Z_wM_q-M_wZ_q)=0 \tag{50}$$

The roots of this equation are

$$\lambda_1,\lambda_2=\tfrac{1}{2}\{M_q+Z_w\pm[(M_q-Z_w)^2+4M_wZ_q]^{\frac{1}{2}}\} \tag{51}$$

Comparing Eqs. (47-49) with Eqs. (50) and (51), a resemblance is noticed. Equation (47) is the first-order term of the characteristic equation, and Eqs. (48) and (49) are the roots of the characteristic equation, all of which are multiplied by the constant $2r/M_{\delta E}^2$. Hence, for the second-order system with single control affecting a single state, the determination of the optimal feedback gains for minimum control energy has a straightforward relationship to the system's open-loop characteristics.

Since we are interested in a statically unstable aircraft, the proper choice for p_{22}/β is given by Eq. (48). Substituting for p_{22}/β in Eq. (45), the slope of the MCE saturation line is given by

$$-p_{12}/p_{22}=\tfrac{1}{2}Z_q\{M_q-Z_w-[(M_q-Z_w)^2+4M_wZ_q]\} \tag{52}$$

This describes the slope of the MCE saturation line for displacement limiting. The slope of the stability boundary, determined earlier to be Eq. (35), is identical to Eq. (52). Thus, it has been shown that the displacement control saturation and stability boundaries are parallel for the second-order MCE system.

Control Rate Limiting

The analytical approach for examining rate limiting was essentially the same as that for displacement limiting. The rate equilibrium point can be predicted using a reduced-order model with the following state equations:

$$\Delta\dot{w}=Z_w\Delta w+Z_q\Delta q \tag{53}$$

$$\Delta\dot{q}=M_w\Delta w+M_q\Delta q+M_{\delta E}\Delta\delta E \tag{54}$$

$$\Delta\dot{\delta}E=\Delta\dot{\delta}E_c \tag{55}$$

A rate-limited elevator command causes a ramp input in elevator position; consequently, Δq and Δw change continually as well. Although the states do not achieve equilibrium, their rates of change approach constant values, as the control-rate limit implies that the time derivative of rate (acceleration) is zero. The equilibrium saddle point is defined by the condition that $\Delta\dot{q}=\Delta\dot{w}=0$, i.e., $d^2q/dw^2=0/0$, and it is denoted by $\Delta\dot{q}^*$and $\Delta\dot{w}^*$. Differentiating Eqs. (53) and (54) and setting them equal to zero leads to

$$\Delta\dot{w}^*=(Z_qM_{\delta E}\Delta\dot{\delta}E)/(Z_wM_q-M_wZ_q) \tag{56}$$

$$\Delta\dot{q}^*=-(Z_wM_{\delta E}\Delta\dot{\delta}E)/(Z_wM_q-M_wZ_q) \tag{57}$$

This is symbolically identical to the displacement saddle-point equation, except that it locates the saddle point in the *state-derivative plane* ($\Delta\dot{q}$-$\Delta\dot{w}$). The saddle point on the stability boundary is given by the solution to Eqs. (56) and (57), for $\Delta\dot{\delta}E=\pm\Delta\dot{\delta}E_{\max}$.

The slopes of the separatices through the saddle points are determined as before. The reduced second-order system for $\Delta\dot{w}$ and $\Delta\dot{q}$ indicates that the stability boundary slope is

$$(\Delta\dot{q}-\Delta\dot{q}^*)/(\Delta\dot{w}-\Delta\dot{w})=\tfrac{1}{2}Z_q\{M_q-Z_w-[(M_q-Z_w)^2+4M_wZ_q]^{\frac{1}{2}}\} \tag{58}$$

which is the same as Eq. (34). Although the initial condition stability boundary is determined in the state-derivative plane ($\Delta\dot{q}$-$\Delta\dot{w}$), it is possible to determine the state-space (Δq-Δw) initial conditions which exceed this boundary using the linear model.

A describing function analysis similar to the displacement limiting analysis can be used for rate limiting as well. The rate-limiting describing function, ρ, is "amplitude depen-

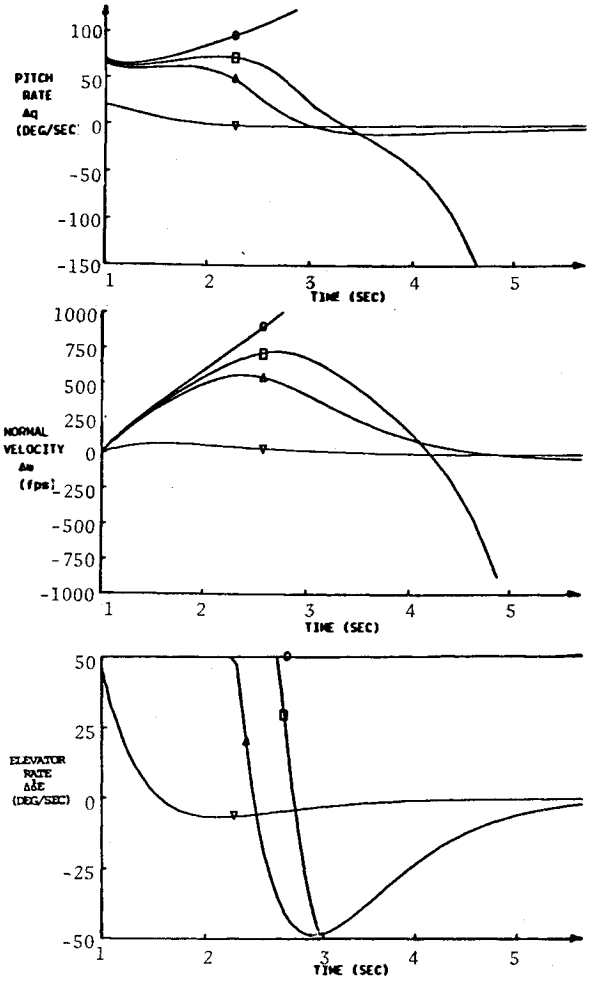

Fig. 6 Response to pitch rate initial conditions (control rate limiting).

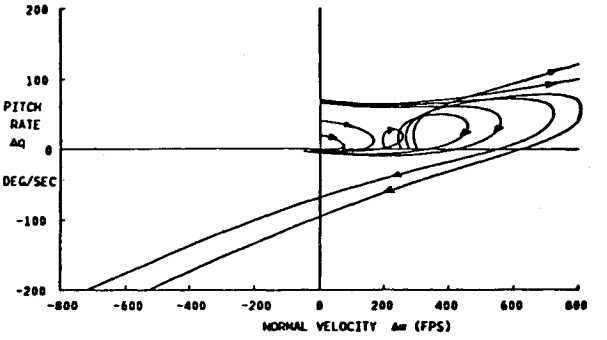

Fig. 7 Projections of state-space trajectories on the Δw-Δw plane (control rate limiting).

dent," i.e., it depends only on the magnitude of the command rate, so the control law is

$$\Delta\delta_R(t) = -\rho[C_x C_\delta]\begin{bmatrix}\Delta x(t)\\ \Delta\delta(t)\end{bmatrix} \tag{59}$$

The sensitivity of ρ_s to control-rate weighting variations is evaluated by uniformly varying the elements of $\boldsymbol{R}_R$ and computing the closed-loop eigenvalues for ρ varying from 0 to 1. $\boldsymbol{R}_R$ was replaced by $\mu\boldsymbol{R}_R$ in Eq. (19), and μ ranged from 0.1 to 500. With $\mu=1$, the diagonal elements of $\boldsymbol{R}_R$ were equal to the inverse elevator and throttle variances used in the displacement analysis. $\boldsymbol{Q}$ also was held constant at its previously mentioned value, Eq. (39). The describing function analysis indicated the same variations as for displacement limiting, with the plot of ρ_s vs μ being essentially identical to Fig. 3. The value of ρ_s was again between 0.2 and 0.5 for μ between 0.1 and 500, with ρ_s limiting at 0.5 for increasing μ. As before, this may appear to imply that low control-rate weighting provides large tolerance to saturation effects, but low control-rate weighting leads to larger feedback gains; saturation occurs for lower levels of the feedback state. Table 2 presents the elevator rate feedback gains, $C^{\delta E}$, for several values of μ. The control laws approach the minimum control energy solutions as μ approaches infinity.

Table 2 illustrates that constant control hyperplanes for various levels of μ *are parallel* in the Δq-Δw plane. For example, $-C_w/C_q = 0.25$ ($\mu=0.1$), and -0.25 ($\mu=500$) (deg/s)/(ft/s); therefore, the hyperplanes are parallel. It follows that if there is a single stability boundary for both control laws, and if it is parallel to one law's control saturation hyperplane, it is parallel to all control saturation hyperplanes.

A comparison of the describing function limiting values with those of the separatrix equations showed that the minimum control energy LQ prediction agrees with those of the separatrix. It is interesting to note that in relation to the initial-condition stability boundary predicted by the saddle point, the describing function limiting values are optimistic for displacement limiting and conservative for rate limiting.

Numerical Analysis

To verify the analysis presented, families of time histories of the response to initial conditions were computed. Attention was directed at the -20% static margin (unstable) case with a $\Delta\delta E_{\max} = \pm 20$ deg displacement limit and a $\Delta\dot{\delta}E_{\max} = \pm 50$ deg/s rate limit. The equations of motion were solved using a fourth-order Runge-Kutta integration with variable time-step intervals.

Control Displacement Limiting

A family of perturbation time histories of the aircraft response to initial conditions was computed. Perturbation time histories for pitch rate initial conditions appear similar to Fig. 4 for all LQ feedback controllers and control displacement weightings examined. The principle differences lie in the location of the linear, unsaturated regions of control.

Time histories for initial pitch rates of 25, 63, and 64 deg/s are shown in the figure. The 25 deg/s case is entirely linear, as the maximum commanded elevator angle is less than 20 deg. Initial pitch rates of 28 deg/s and above cause the elevator control to saturate, although the response remains stable for initial pitch rates up to 63 deg/s (also shown). In such case, the system is nonlinear but *piecewise linear,* with a discrete change in dynamic characteristics at the control saturation boundary. The elevator saturation persists for 2 s; nevertheless, the aircraft's stabilizing pitch rate and heave damping overpower the destabilizing effect of the negative static margin, allowing a capture in the region of unsaturated control.

For an initial pitch rate of 64 deg/s, the static instability is dominant. The control remains saturated, and the state variables diverge. Clearly, the stability boundary lies between initial pitch rates of 63 and 64 deg/s.

Further insight regarding the response phenomenon, and the validity of the saddle-point analysis can be gained by examining the *projections* of the corresponding trajectories in the Δq-Δw plane. The resulting plots are analogous to the familiar phase-plane "portraits" for low-order nonlinear systems,[9,10] but state variables rather than phase variables are employed. It also must be kept in mind that the trajectory actually falls outside the Δq-Δw plane and is sensitive to the values of state variables that do not appear in the trajectory's projection. For example, two trajectories beginning with the

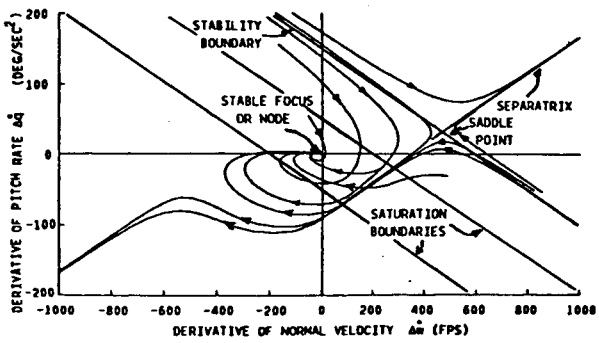

Fig. 8 Projections of state-derivative trajectories on the Δq-$\Delta \dot{w}$ plane (control rate limiting).

same initial Δq and Δw do not have the same Δq-Δw projection if the initial Δu and $\Delta\theta$ are different.

Figure 5 presents a number of Δq-Δw traces for various initial conditions. Five histories begin with increasing values of Δq, and all the other initial state perturbations equal to zero. An additional five begin with $\Delta w = 400$ ft/s and decreasing values of Δq_o. The trajectory projections form well-organized patterns that are analogous to phase-plane plots for second-order systems. The predicted *saddle point* appears in the upper right quadrant, and there is a *stable focus or node* at the origin. By symmetry, a second saddle point would appear in the lower left quadrant for trajectories with the appropriate initial conditions.

The *intersections* (not projections) of the control saturation hyperplanes for $\mu = 1$ also are shown. A stable region that is outside and essentially parallel to the saturation line can be identified. The stability boundary is defined by a straight line that intersects the vertical axis at $\Delta w = 63.5$ deg/s and the horizontal axis at $\Delta w = 260$ ft/s. Initial conditions which fall outside this boundary result in divergence. Trajectories that originate near the stability boundary approach the saddle point, then split off for either convergent or divergent response along the separatrix emanating from the saddle point.

The intersections of the defined stability boundaries with the Δq-Δw axes are essentially those predicted by the separatrices of the second-order system. This complements and verifies the use of the reduced-order model for determination of the stability boundary imposed by control displacement saturation. The minimum control energy describing function also approximates the same limiting values; hence, the describing function formulation is appropriate.

Control Rate Limiting

The rate-limited aircraft control model was used to compute a family of perturbation time histories of the aircraft's response to initial conditions. Figure 6 presents time histories for initial pitch rates Δq of 20, 65, 67.5, and 70 deg/s. The 20 deg/s case is entirely linear, since the maximum commanded elevator rate is less than 50 deg/s. Elevator rate saturation occurs for initial pitch rates of 22 deg/s and above, although the response remains stable to 65 deg/s (also shown). At $\Delta q = 65$ deg/s, the aircraft's stabilizing pitch rate and heave damping overpower the destabilizing effect of the negative static margin. The Δq trace shows an initial oscillatory response while the elevator rate is saturated, with the change in the pitch rate dynamic characteristic at the saturation boundary.

As seen in Fig. 6, the stability boundary lies between initial pitch rates of 65 and 67.5 deg/s. For $\Delta q = 67.5$ deg/s, the aircraft's pitch rate begins returning to zero; however, this reversal does not lead to a stable situation or capture. As the pitch rate decreases and passes through zero, the elevator is rate limited in its motion, and it cannot decrease rapidly enough to stop the increasing negative pitch rate. With the elevator in a positive deflection, it drives the aircraft's pitch rate toward further increasing negative pitch rate. The aircraft diverges in the direction opposite to its initial condition. For an initial pitch rate of 70 deg/s, the static instability is dominant. This time the control remains saturated at 50 deg/s, and the state variables diverge in the same direction as the initial condition.

Figure 7 is a plot of a number of Δq-Δw traces for various Δq and Δw initial conditions. These trajectories do not form well-organized patterns as they did for the displacement limiting case. This is not surprising, recalling that the saddle-point prediction defines the equilibrium point in the state-derivative plane.

The corresponding plot in the Δq-$\Delta \dot{w}$ plane is presented in Fig. 8. The trajectories form the well-organized patterns seen in Fig. 5. The two types of equilibrium points are apparent in the figure. There is a *stable focus or node* at the origin and a *saddle point* in the upper right quadrant. By symmetry, a second saddle point would appear in the lower left quadrant for trajectories with the appropriate initial conditions. As before, the trajectories fall outside of the plane and are sensitive to the values of state variables which do not appear in the trajectory's projection. This is especially true if the initial elevator state $\Delta\delta E$ is markedly different.

The intersections of the control-rate saturation hyperplanes for $\mu = 1$ also are shown in Fig. 8. The stability boundary is defined by a straight line that intersects the vertical axis at $\Delta \dot{q} = 160$ deg/s^2 and the horizontal axis at $\Delta \dot{w} = 640$ ft/s^2. The stability boundary-axis intersections are predicted by the saddle-point separatrix analysis to be at $\Delta \dot{q} = 159$ deg/s^2 and $\Delta \dot{w} = 637$ ft/s^2. This verifies the reduced-order saddle-point analysis, as well as the use of the state-derivative plane for initial condition stability predictions.

Conclusion

Novel analytical techniques for examining and interpreting the effects of control displacement and rate saturation on longitudinal stability have been developed and applied to a generic lightweight fighter aircraft with static instability. The utility of using reduced-order models for characterizing the regions of stable or satisfactory response is shown. The equilibrium points of the reduced-order models are used to predict the regions of instability. The regions of instability also are estimated using a quasilinear approach, in which the saturation nonlinearities are replaced by describing functions. Using the reduced-order models, the control saturation and stability hyperplanes are shown to be parallel for the minimum control energy-quadratic control solutions and either displacement or rate limiting. The stability boundary is independent of the weighting matrices of a linear-quadratic cost function and is closely predicted by both the equilibrium point and minimum control energy describing function analyses. A direct relation between the minimum control energy LQ control solution and the open-loop characteristics of the aircraft also is shown. These results have direct application in the design of stability augmentation systems for future aircraft.

Acknowledgments

This research has been sponsored by NASA Langley Research Center under Grant NSG 1587.

References

[1] Lapins, M., Klein, R. W., Martorella, R. P., and Meyer, R. C., "Impact of Relaxed Static Stability on Flight Control and Handling Qualities of Advanced Supersonic Tactical Fighters," Tactical Aircraft Research and Technology Conference, Hampton, Va., 1980.

[2] Rynaski, E. G. and Weingarten, N. C., "Flight Control Principles for Control Configured Vehicles," AFFDL-TR-71-154, Jan. 1972.

[3]Hanson, G. D., "Command and Stability Augmentation Techniques for Aircraft with Control Saturation," M.S.E. Thesis, Princeton University, Princeton, N.J., 1981.

[4]Stengel, R. F., "Equilibrium Response of Flight Control Systems," *Automatica,* Vol. 18, No. 3, May 1982, pp. 343-348.

[5]Kalman, R. E., "Contributions to the Theory of Optimal Control," *Bol. Soc. Mat. Mexicana,* Vol. 5, 1960, pp. 102-119.

[6]Vidyasgar, M., *Nonlinear Systems Analysis,* Prentice-Hall, Inc., Englewood Cliffs, N.J., 1978.

[7]Gelb, A. and VanderVelde, W. B., *Multiple-Input Describing Functions and Nonlinear System Design,* McGraw-Hill Book Co., New York, 1968.

[8]Safonov, M. G. and Athans, M., "Gain and Phase Margins for Multiloop LQG Regulators," IEEE *Transactions on Automatic Control,* Vol. AC-22, No. 2, April 1977, pp. 173-179.

[9]Gibson, J. E., *Nonlinear Automatic Control,* McGraw-Hill Book Co., New York, 1963.

[10]Graham, D. and McRuer, D., *Analysis of Nonlinear Control Systems,* John Wiley & Sons, New York, 1961.

[11]Hanson, G. D., and Stengel, R. F., "Effects of Control Saturation on the Command Response of Statically Unstable Aircraft," AIAA Paper No. 83-0065, Jan. 1983.